

Survival of the Scarcer in Space

Renato Vieira dos Santos

Departamento de Física, Instituto de Ciências Exatas,
Universidade Federal de Minas Gerais, CP 702, CEP 30161-970,
Belo Horizonte, Minas Gerais, Brasil.

e-mail: *econofisico@gmail.com*

Ronald Dickman

Departamento de Física, Instituto de Ciências Exatas,
and National Institute of Science and Technology for Complex Systems,
Universidade Federal de Minas Gerais, CP 702, CEP 30161-970,
Belo Horizonte, Minas Gerais, Brasil.

April 12, 2013

Abstract

Recently a model of intra- and interspecific competition between two species was proposed [Phys. Rev. E 87 (2013) 010101], in which the scarcer species (i.e., with smaller stationary population size) can be more resistant to extinction when it holds a competitive advantage. Here we verify this survival of the scarcer in space (SSS) phenomenon in models with spatial structure, both analytically and numerically. We find that the conditions for SSS, as obtained applying renormalization group analysis and Monte Carlo simulation to a discrete-space model, differ significantly from those found in the spatially homogeneous case.

Keywords: Demographic stochasticity, Doi-Peliti mapping, Renormalization group, Monte Carlo simulation.

1 Introduction

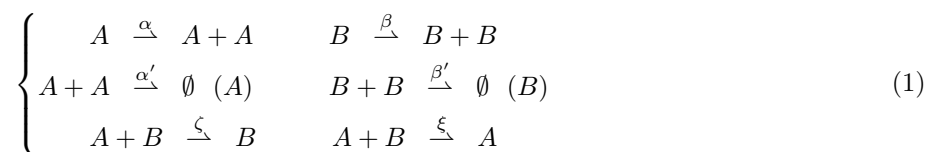
Recently, Gabel, Meerson, and Redner [1] proposed a stochastic model of two-species competition in which, for stationary regimes such that the two species coexist, the scarcer species (i.e., with smaller population size), can, under certain conditions, be less susceptible to extinction than the more populous species. This phenomenon, dubbed *survival of the scarcer* (SS) in [1], is surprising since conventional wisdom on population dynamics suggests that a smaller population is more susceptible to extinction due to demographic fluctuations. The authors of [1] use a variant of the Wentzel-Kramers-Brillouin-Jeffreys (WKBJ) approximation to obtain the tails of the quasi-stationary probability distribution of the process [2, 3]. They show that a small asymmetry in interspecific competition can induce survival of the scarcer species.

While the analysis of [1] holds for well mixed (spatially uniform) populations, it is natural to inquire whether the same conclusions apply for populations distributed in space. In this paper we study a stochastic model similar to that of [1], but with organisms located on a d -dimensional lattice, and investigate the conditions required for survival of the scarcer in space (SSS). On reproduction, a daughter organism appears at the same site as the mother; competition only occurs between organisms at the same site. In addition to these reactions, organisms also diffuse on the lattice. Starting from the master equation, we build a representation involving creation and annihilation operators, taking advantage of the discrete nature of the stochastic process. This representation allows us to obtain a full functional integral formulation, which can be regarded as a mapping of the stochastic process to a field theory. This now standard procedure is known as the Doi-Peliti mapping [4, 5, 6]. We consider the population dynamics in a critical situation, i.e., populations close to extinction. The dynamic renormalization group (DRG) is used to study the nonequilibrium critical dynamics of the population dynamics, specifically, to determine how the model parameters transform under changes in length and time scales. The model is also studied via Monte Carlo simulation, which again confirms the existence of SSS when the less populous species is more competitive.

The remainder of this paper is organized as follows. In section 2 we describe the model and write the effective action associated with the stochastic process. A brief analysis of mean-field theory, valid in dimensions greater than the critical dimension is performed. In section 3 we use some known results on multispecies directed percolation to obtain the renormalization group flow in parameter space. This analysis, combined with numerical simulations of the associated stochastic partial differential equations, allow us to determine the regions in parameter space in which SSS occurs. Results of Monte Carlo simulations are presented in Section 4. Section 5 closes the paper with our conclusions.

2 Model

The model proposed in [1] may be described, with some minor modifications in the rates as specified below, by the following set of reactions:



The reactions in the first line correspond to reproduction of species A and B . Those in the second line describe intraspecific competition processes which may be of mutual annihilation (\emptyset) or individual death (A/B), while the third line represents interspecific competition. α (β), α' (β') and ζ (ξ) are the rates of the reactions associated with species A (B).

The relation between the rates in equation (1) and those of the original model [1] is (in the case of mutual annihilation): $\alpha \leftrightarrow 1$, $\beta \leftrightarrow g$, $\alpha' \leftrightarrow 1/K$, $\beta' \leftrightarrow 1/K$, $\zeta \leftrightarrow \epsilon/K$, and $\xi \leftrightarrow \delta\epsilon/K$. $\delta < 1$ implies an asymmetry in competition between species that favors B at expense of A . In this case species B is *more competitive* than A ; the opposite occurs if $\delta > 1$.

The authors of Ref. [1] constructed a phase diagram in the g - δ plane (shown schematically in Figure 1). The phase diagram includes results of both mean-field theory (MFT) and analysis of the master equation for a

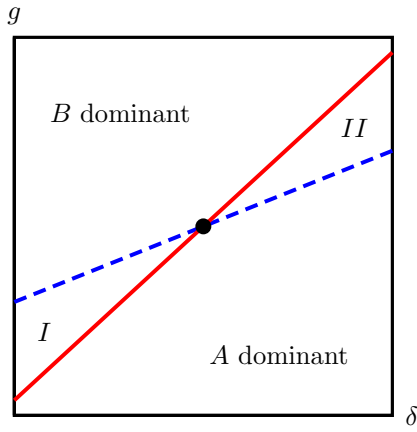


Figure 1: Phase diagram of well mixed system in the g - δ plane, as furnished by the analysis of Ref. [1]. Dashed blue curve: $g_{mf} = (1 + \delta\epsilon)/(1 + \epsilon)$. Full red curve: $g_{sw} = (1 + m\delta\epsilon)/(1 + m\epsilon)$.

stochastic population model in a well mixed system, i.e., without spatial structure. In MFT, the populations of the two species are equal when $g_{mf}(\delta) = (1 + \delta\epsilon)/(1 + \epsilon)$. Analysis of the master equation yields equal extinction probabilities when $g_{sw}(\delta) = (1 + m\delta\epsilon)/(1 + m\epsilon)$ with $m \equiv [(\ln 2)^{-1} - 1]^{-1}$. These conditions are plotted in figure 1; they intersect at the point $(g, \delta) = (1, 1)$. The phase diagram includes two “normal” regions, in which the more populous species is less likely to go extinct, and two “anomalous” regions, in which the scarcer species is more likely to survive. Thus in region *I* (where $\delta < 1$ and *B* is more competitive in the sense defined above), species *A* is more numerous in the quasi-stationary state and simultaneously more susceptible to extinction, while in region *II* (where $\delta > 1$ and *A* is more competitive), species *B* is more numerous, yet more likely to go extinct first. Regions *I* and *II* are anomalous since they correspond to an inversion of the usual dictum that susceptibility to extinction grows with diminishing population size. Our goal in this work is to determine whether a stochastic model of two-species competition with spatial structure, in which organisms diffuse in d -dimensional space, exhibits a similar phenomenon. In the following subsection we develop a continuum description for this spatial stochastic process.

2.1 Effective action

We consider a stochastic implementation of the reactions of equation (1) on a d -dimensional lattice, adding diffusion (nearest-neighbor hopping) of individuals of species *A* and *B* at rates D_A and D_B respectively. Following the standard Doi-Peliti procedure mentioned in the Introduction, ignoring irrelevant terms (in the renormalization group sense) and with the so-called Doi shift [6] already performed, we obtain the following effective action:

$$\begin{aligned}
S(\bar{\phi}, \phi, \bar{\psi}, \psi) &= \int d^d x \int dt \{ \bar{\phi} [\partial_t + D_A(\sigma_A - \nabla^2)] \phi - \alpha \bar{\phi}^2 \phi + j \alpha' \bar{\phi} \phi^2 + \alpha' \bar{\phi}^2 \phi^2 + \zeta \psi \phi \bar{\phi} \} \\
&+ \int d^d x \int dt \{ \bar{\psi} [\partial_t + D_B(\sigma_B - \nabla^2)] \psi - \beta \bar{\psi}^2 \psi + j \beta' \bar{\psi} \psi^2 + \beta' \bar{\psi}^2 \psi^2 + \xi \phi \psi \bar{\psi} \}, \quad (2)
\end{aligned}$$

where $\sigma_A \equiv -\alpha/D_A$, $\sigma_B \equiv -\beta/D_B$ and $j \equiv 1$ (2) for individual death (mutual annihilation). Action S has four fields. The expected values of the fields ϕ and ψ (evaluated by performing functional integrals over the four fields, using the weight $\exp[-S]$), represent the mean population densities of species *A* and *B*, respectively. The fields with overbars have no immediate physical interpretation, but are related to intrinsic fluctuations of

the stochastic dynamics.

Using the definitions of σ_A and σ_B and the change of variable $\bar{\phi} \rightarrow \theta_A \bar{\phi}$, $\phi \rightarrow \theta_A^{-1} \phi$, $\bar{\psi} \rightarrow \theta_B \bar{\psi}$, and $\psi \rightarrow \theta_B^{-1} \psi$, where $\theta_A \equiv \sqrt{\frac{j\alpha'}{\alpha}}$, $\theta_B \equiv \sqrt{\frac{j\beta'}{\beta}}$, we can write the effective action in the form:

$$\begin{aligned}
S(\bar{\phi}, \phi, \bar{\psi}, \psi) &= \int d^d x \int dt \left\{ \bar{\phi} [\partial_t + D_A(\sigma_A - \nabla^2)] \phi \right. \\
&+ \bar{\psi} [\partial_t + D_B(\sigma_B - \nabla^2)] \psi \\
&+ g_A \bar{\phi} (\phi - \bar{\phi}) + g_B \bar{\psi} (\psi - \bar{\psi}) \\
&\left. + h_B \phi \bar{\psi} + h_A \phi \bar{\phi} \right\}, \tag{3}
\end{aligned}$$

with

$$\begin{cases} g_A \equiv \sqrt{j\alpha\alpha'} \\ h_A \equiv \theta_A^{-1} \zeta \\ g_B \equiv \sqrt{j\beta\beta'} \\ h_B \equiv \theta_B^{-1} \xi. \end{cases} \tag{4}$$

Dimensional analysis yields,

$$[h_A] = [h_B] = p^{2-\frac{d}{2}} = [g_A] = [g_B],$$

where $[X]$ denotes the dimensions of X , and p has dimensions of momentum [6]. The upper critical dimension is therefore $d_c = 4$, as for single-species processes such as the contact process and directed percolation.

2.2 Mean-field approximation

For $d \geq d_c$, mean-field analysis, which ignores fluctuations in ϕ and ψ , yields the correct critical behavior.

Imposing the conditions $\frac{\delta S}{\delta \bar{\phi}} = 0$, $\frac{\delta S}{\delta \bar{\psi}} = 0$, $\frac{\delta S}{\delta \phi} = 0$ and $\frac{\delta S}{\delta \psi} = 0$, we obtain the mean-field equations

$$\begin{cases} \frac{\partial \phi}{\partial t} = D_A \nabla^2 \phi + \alpha \phi - g_A \phi^2 - h_B \phi \bar{\psi} \\ \frac{\partial \psi}{\partial t} = D_B \nabla^2 \psi + \beta \psi - g_B \psi^2 - h_A \phi \bar{\phi}. \end{cases} \tag{5}$$

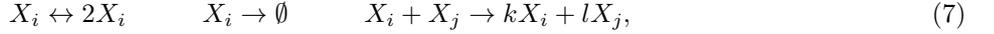
Let L be a typical length scale and define $X = g_A \phi / \alpha$, $Y = g_B \psi / \beta$, $s = D_A t / L^2$, and define a rescaled coordinate $x' = x / L$. Then equation (5) can be written in dimensionless form as

$$\begin{cases} \frac{\partial X}{\partial s} = \nabla^2 X + \gamma (X - X^2 - aXY) \equiv \nabla^2 X + f(X, Y) \\ \frac{\partial Y}{\partial s} = D \nabla^2 Y + \gamma (cY - cY^2 - bXY) \equiv D \nabla^2 Y + g(X, Y) \end{cases} \tag{6}$$

with $\gamma \equiv \alpha L^2 / D_A$, $a \equiv \beta h_B / (\alpha g_B)$, $b \equiv \beta h_A / (\alpha g_B)$, $c \equiv g_A \beta^2 / (g_B \alpha^2)$, $D \equiv D_B \beta g_A / (D_A \alpha g_B)$, $f(X, Y) \equiv \gamma (X - X^2 - aXY)$ and $g(X, Y) \equiv \gamma (cY - cY^2 - bXY)$. Coexistence is possible in the stationary state if the conditions $c > b$ and $a < 1$ hold, implying $h_A < \beta g_A / \alpha$ and $h_B < \alpha g_B / \beta$. These conditions depend monotonically on parameters α , β , g_A and g_B , analogous to the coexistence conditions found in [1]. The same is not true in spatial stochastic theory, as we shall see in the next section.

3 Renormalization group (RG) flow

Some years ago, Janssen analyzed a class of reactions of the kind defined in equation (1) [7]. This work considered multi-species reactions of the form



where i and j are species indices and k, l are either zero or unity; this process is called *multicolored directed percolation* (MDP), with different colors referring to different species. The RG analysis of [7] shows that knowledge of the directed percolation fixed points is sufficient to determine the fixed points of the full MDP. As shown in that work, the parameter combinations $g_A/D_B \equiv u_A$ and $g_B/D_A \equiv u_B$, related to intraspecific competition, flow under renormalization group transformations to the stable DP fixed point $u_A^* = u_B^* = u^* = 2\epsilon/3$ with $\epsilon = 4 - d > 0$.¹ Therefore, regarding the renormalization of intraspecific competition parameters, inclusion of other species behaving as in DP does not alter the fixed point.

Janssen's analysis shows that there are four fixed points for interspecific competition parameters $h_A/D_A \equiv v_A$ and $h_B/D_B \equiv v_B$, which from reactions (1) are related to ξ and ζ . The first two are $(v_A^*, v_B^*) = (0, 0)$, which is unstable, and

$$(v_A^*, v_B^*) = \left(\frac{D_A + D_B}{D_A} \frac{2}{3} \epsilon, \frac{D_A + D_B}{D_B} \frac{2}{3} \epsilon \right) \quad (8)$$

which is a hyperbolic fixed point if $D_A = D_B$.² For $D_A \neq D_B$, it was conjectured [7] that the stability of the fixed points remains the same despite small changes in the renormalization group flow diagram topology. The other two fixed points for $D_A = D_B$ are stable; they are given by $(v_A^*, v_B^*) = (0, 2u^*)$ and $(v_A^*, v_B^*) = (2u^*, 0)$. To summarize, for $D_A = D_B \equiv D_0$, the interspecies competition parameters flow to one of the following four d -dependent fixed points (denoted as **O**, **F**, **G**, and **H** below),

$$\begin{aligned} (v_A, v_B) &= \left(\frac{\theta_A^{-1} \zeta}{D_0}, \frac{\theta_B^{-1} \xi}{D_0} \right) \\ &\rightarrow \left\{ \begin{array}{l} \mathbf{O} : (0, 0), \quad \mathbf{F} : (u^*, u^*), \\ \mathbf{G} : (2u^*, 0), \quad \mathbf{H} : (0, 2u^*) \end{array} \right\} \end{aligned} \quad (9)$$

Figure 2 shows the renormalization group flow diagram. The unstable fixed point **O** corresponds to complete decoupling between the two species, and the hyperbolic point **F** to symmetric coupling. In the symmetric subspace, any nonzero initial value of $v \equiv v_A = v_B$, flows to **F**. For $v_B > v_A$ ($\delta > 1$), (v_A, v_B) flows to **G**, so that species A is effectively unable to compete with B . Similarly, if $v_A > v_B$ ($\delta < 1$), the flow attains point **H**. In the following subsection we discuss the stationary states associated with these fixed points.

¹Not to be confused with parameter ϵ used in equation 1.

²In the nomenclature of [7], if species are of the same flavor.

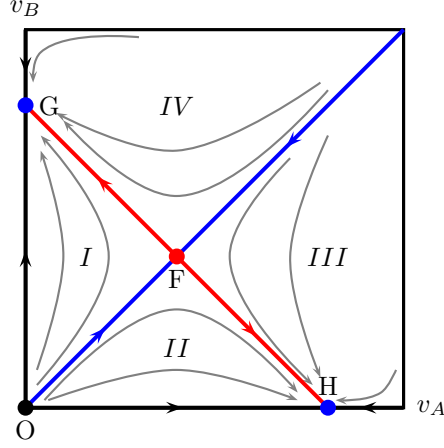


Figure 2: RG flow of the interspecific competition parameters v_B and v_A . Only the first quadrant is relevant due to the requirement of positive rates. There is an unstable fixed point \mathbf{O} at $(v_A, v_B) = (0, 0)$ (black dot); a hyperbolic fixed point \mathbf{F} at $(v_A, v_B) = (u^*, u^*)$ (red dot), and two stable fixed points \mathbf{G} and \mathbf{H} , located at $(v_A, v_B) = (0, 2u^*)$ and $(v_A, v_B) = (2u^*, 0)$ respectively (blue dots). The separatrix $v_A = v_B$ is the boundary between the basins of attraction of \mathbf{G} and \mathbf{H} .

3.1 Steady state close to critical points

Population dynamics in the critical regime is governed by a pair of coupled stochastic partial differential equations (SPDE), which are readily deduced from the action of equation (3)[8]:

$$\frac{\partial \phi}{\partial t} = D_0 \nabla^2 \phi + \alpha \phi - g_A \phi^2 - h_B \phi \psi + \eta_1 \quad (10)$$

and

$$\frac{\partial \psi}{\partial t} = D_0 \nabla^2 \psi + \beta \psi - g_B \psi^2 - h_A \psi \phi + \eta_2 \quad (11)$$

where the noise terms $\eta_1(\mathbf{x}, t)$ and $\eta_2(\mathbf{x}, t)$ satisfy $\langle \eta_1(\mathbf{x}, t) \rangle = \langle \eta_2(\mathbf{x}, t) \rangle = 0$, and

$$\langle \eta_1(\mathbf{x}, t) \eta_1(\mathbf{x}', t') \rangle = 2g_A \phi(\mathbf{x}, t) \delta^d(\mathbf{x} - \mathbf{x}') \delta(t - t'), \quad (12)$$

$$\langle \eta_2(\mathbf{x}, t) \eta_2(\mathbf{x}', t') \rangle = 2g_B \psi(\mathbf{x}, t) \delta^d(\mathbf{x} - \mathbf{x}') \delta(t - t'). \quad (13)$$

Note that these multiplicative noise terms depend on the square root of their respective fields, and were obtained directly from the action, without any additional hypotheses.

3.1.1 SPDE in the vicinity of point \mathbf{F}

In the symmetric subspace, $\delta = 1$, the RG flow is to the fixed point \mathbf{F} , and parameters g_A/D_0 , g_B/D_0 , h_A/D_0 , and h_B/D_0 take the associated values. Therefore the SPDEs in (10) and (11) can be written as [9]:

$$\frac{\partial \phi}{\partial t} = D_0 \nabla^2 \phi + \phi - D_0 u^* \phi^2 - D_0 u^* \phi \psi + \eta_1, \quad (14)$$

$$\frac{\partial \psi}{\partial t} = D_0 \nabla^2 \psi + g\psi - D_0 u^* \psi^2 - D_0 u^* \psi \phi + \eta_2 \quad (15)$$

where we set $\alpha = 1$ and $\beta = g$. With the rescaling $\phi \rightarrow \phi/(D_0 u^*)$, $\psi \rightarrow \psi/(D_0 u^*)$ and $x \rightarrow (1/D_0)^{1/2} x$, we can write equations (14) and (15) in the form:

$$\frac{\partial \phi}{\partial t} = \nabla^2 \phi + \phi - \phi^2 - \phi \psi + \eta_1, \quad (16)$$

$$\frac{\partial \psi}{\partial t} = \nabla^2 \psi + g\psi - \psi^2 - \psi \phi + \eta_2 \quad (17)$$

with rescaled noise

$$\langle \eta_1(\mathbf{x}, t) \eta_1(\mathbf{x}', t') \rangle = 2 (D_0)^{2-\frac{d}{2}} (u^*)^2 \phi(\mathbf{x}, t) \delta^d(\mathbf{x} - \mathbf{x}') \delta(t - t') \quad (18)$$

$$\langle \eta_2(\mathbf{x}, t) \eta_2(\mathbf{x}', t') \rangle = 2 (D_0)^{2-\frac{d}{2}} (u^*)^2 \psi(\mathbf{x}, t) \delta^d(\mathbf{x} - \mathbf{x}') \delta(t - t'). \quad (19)$$

For $d < 4$, the rescaled noise intensity σ grows with diffusion rate D_0 ; for $d = 1$ we have $\sigma^2 = 2D_0^{\frac{3}{2}} u^{*2}$ with $u^{*2} \approx 2$. Figures 3(a) and 3(b) show results of numerical simulations of equations (16) and (17) in $d = 1$ with $g = 1$. They show, for a one-dimensional lattice of $L = 128$ sites in the interval $(-1, 1)$, the population densities averaged over 1000 Monte Carlo realizations for two different values of the noise intensity. The time interval T is $T = 400$, partitioned into $N = 40000$ steps so that $\Delta t \equiv T/N = 400/40000 = 0.01$. Initial conditions are $\phi(x, 0) = 0.4$ and $\psi(x, 0) = 0.6$. For $\sigma = 0$, population densities are almost time-independent as shown in Figure 3(a). This is not the case for larger noise values. In this case, the two populations tend to the same value (see figure 3(b)). Although Figs. 3(a) and 3(b) represent averages over many realizations, we have verified coexistence in individual runs.

These simulations were performed using standard integration techniques for the Langevin equation with the XMDS2 software [10]. Since we are interested in showing only the initial temporal trends of the two population densities in the vicinity of fixed points, the use of standard techniques of integrating the Langevin equations is sufficient to reveal the qualitative nature of the solutions. Near a phase transition to an absorbing state, one of the population densities tends to zero and the standard numerical integration scheme fails. This standard algorithm is not suitable for extracting the more accurate results associated with critical exponents or asymptotic decays. In this case we would have to use more sophisticated algorithms such as those proposed in [11, 12, 13].

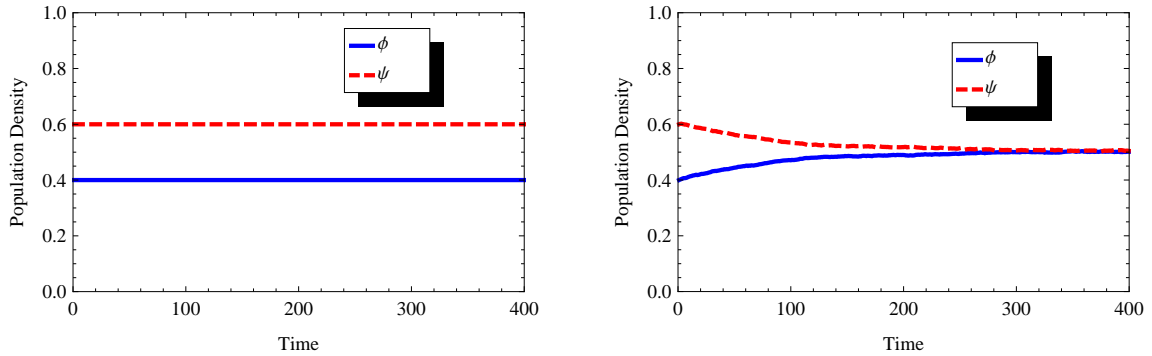
3.1.2 SPDE in the vicinity of a stable fixed point

Now consider the case $\delta \neq 0$. With $\delta > 1$, the parameters flow to point \mathbf{G} and Eqs. (10) and (11) become

$$\frac{\partial \phi}{\partial t} = D_0 \nabla^2 \phi + \phi - u^* \phi^2 + \eta_1, \quad (20)$$

$$\frac{\partial \psi}{\partial t} = D_0 \nabla^2 \psi + g\psi - u^* \psi^2 - 2u^* \psi \phi + \eta_2, \quad (21)$$

where we put $\alpha = 1$ and $\beta = g$. With a rescaling similar to that used above, we have



(a) Symmetric case with $\sigma = 0.0$ and $g = 1$. Initial populations are $\phi(x, 0) = 0.4$ and $\psi(x, 0) = 0.6$. (b) Symmetric case with $\sigma = 0.03$ and $g = 1$. Initial populations are $\phi(x, 0) = 0.4$ and $\psi(x, 0) = 0.6$.

Figure 3: Numerical simulations symmetric SPDE.

$$\frac{\partial \phi}{\partial t} = \nabla^2 \phi + \phi - \phi^2 + \eta_1, \quad (22)$$

$$\frac{\partial \psi}{\partial t} = \nabla^2 \psi + g\psi - \psi^2 - 2\phi\psi + \eta_2 \quad (23)$$

with η_1 and η_2 satisfying (18) and (19), respectively. For $\delta < 1$ the situation is completely analogous to the case $\delta > 1$, and the resulting equations are as above with the exchange of ϕ and ψ and changing the position of the factor g accordingly.

If we neglect diffusion and noise terms, we have a system of ordinary differential equations having a fixed point associated with the stable coexistence state given by $(\phi^*, \psi^*) = (1, g - 2)$.³ Therefore, the condition for coexistence is $g > 2$. If $g < 2$, only species A survives for $\delta > 1$. Figure (4) shows the result of a simulation with $g = 2.2$ in which the equations are integrated including both diffusion and noise. Numerical experiments indicate that the effect of these terms is to increase the value of $g \gtrsim 2$ for coexistence. Higher noise values imply higher thresholds g for coexistence.

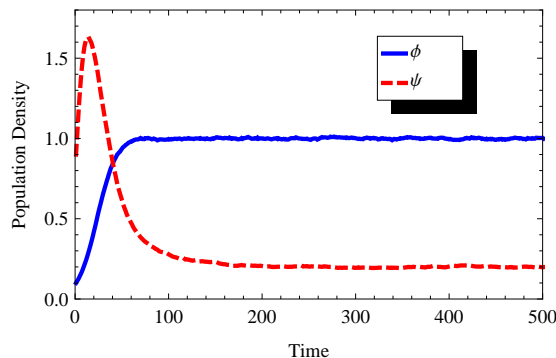


Figure 4: Asymmetric case ($\delta = 1.5$) with $\sigma = 0.03$ and $g = 2.2$. Initial populations for A and B species are $\phi(x, 0) = 0.1$ and $\psi(x, 0) = 0.9$, respectively.

For $\delta < 1$ similar reasoning applies. The results are summarized in the phase diagram of Fig. 5. There are four stationary phases: a pure- A phase for $\delta > 1$ and $g < 2$, a symmetric pure- B phase for $\delta < 1$ and $g < 1/2$, and two (disjoint) coexistence phases. The latter arise when the less competitive species proliferates sufficiently faster than the more competitive one.

³For the case $\delta < 1$, fixed points are $(\phi^*, \psi^*) = (1 - 2g, g)$, and coexistence condition is $0 < g < 1/2$.

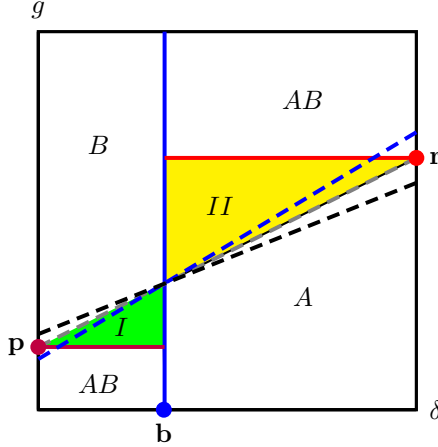


Figure 5: Stationary phase diagram in the g - δ plane for stochastic model with spatial structure. The reference points have coordinates: $\mathbf{b} = (1, 0)$, $\mathbf{p} = (0, 1/2)$, $\mathbf{r} = (3, 2)$. For $\delta > 1$, when $g < 2$ only species A is present, while for $g > 2$ there is coexistence. Similarly, for $\delta < 1$, when $g > 1/2$ only species B is present, and for $g < 1/2$ there is coexistence. The diagonal line connecting points \mathbf{p} and \mathbf{r} is the equal-population criterion furnished by mean-field theory, $g_{mf}(\delta) = (1 + \epsilon\delta)/(1 + \epsilon)$, with $\epsilon = 1$. In regions I and II , the more populous species (A or B , respectively), as predicted by mean-field theory, in fact goes extinct. The thick, dashed, blue and black curves represent g_{mf} and g_{sw} for the value of ϵ that maximizes the area between them, i.e., $\epsilon = 1/\sqrt{m} \approx 0.66$.

3.1.3 Nature of phase transitions

From the equations that omit the diffusion and noise terms, one may infer the nature of the phase transitions in the diagram of Fig. (5). From Table 1, which shows the fixed points of the equations for different values of δ , we see that in general the values in the final column do not match for $\delta \neq 1$. This fact indicates that the vertical blue

Table 1: Simplified equations and their fixed points for different values of δ

δ	Equation	Fixed Point
$= 1$	$\dot{\phi} = \phi - \phi^2 - \phi\psi$ and $\dot{\psi} = g\psi - \psi^2 - \phi\psi$	$(\phi^*, \psi^*) = (0, g)$
> 1	$\dot{\phi} = \phi - \phi^2$ and $\dot{\psi} = g\psi - \psi^2 - 2\phi\psi$	$(\phi^*, \psi^*) = (1, 2 - g)$
< 1	$\dot{\phi} = g\phi - \phi^2$ and $\dot{\psi} = \psi - \psi^2 - 2\phi\psi$	$(\phi^*, \psi^*) = (g, 1 - 2g)$

line in the diagram (5), i.e., the line $\delta = 1$, is a line of discontinuous phase transitions. Similarly, examining the expressions in the final column of Table 1, we infer the nature of phase transitions along the horizontal lines at $g = 1/2$ and $g = 2$. In regions of coexistence, the densities of the minority species grow continuously from zero; thus these transitions are continuous. One should of course recognize that the predictions for the phase diagram are essentially qualitative; quantitative predictions for nonuniversal properties such as phase boundaries are not possible once irrelevant terms have been discarded. Regarding the nature of the transitions, we expect the continuous ones, as furnished by this mean-field-like analysis, to in fact belong to the DP universality class [7]. The line of discontinuous transitions contains a portion (between levels \mathbf{p} and \mathbf{r}) that is between absorbing subspaces (only on species present in each phase), and other portions that separate (from the viewpoint of the species undergoing extinction) an active and an absorbing phase. Discontinuous transitions of this nature are not expected to occur in one dimension [14].

According to mean-field theory, a point in region II corresponds to $\rho_B > \rho_A$. If we increase the competitiveness of species A , increasing δ while maintaining g fixed, there will be a point beyond which species B no

longer has the greater population density. Improvement of the competitiveness of species A will make it the more populous species if organisms are well mixed. In the case of a spatially structured population, by contrast, *any* competitive advantage of species A , no matter how small, is sufficient to dominate the B population (if the latter does not proliferate very rapidly) when the population densities are very low, as is the case near criticality. Thus in a situation in which mean-field theory predicts species B to be the majority, we can have species A *exclusively*. This can be seen as a strong version of the survival of the scarcer phenomenon.

To compare the predictions of the mean-field and spatially structured descriptions, a pair of dashed lines are plotted in Fig. 5, representing equations for g_{mf} and g_{sw} as defined previously, for parameters such that the area between them is maximum, thereby maximizing the region in which SS occurs. [The maximum area is obtained using $\epsilon = 1/\sqrt{m}$ with $m = [(\ln 2)^{-1} - 1]^{-1}$, in Eq. (1)]. Given the much larger area of the region exhibiting SS in the spatial model, compared with that in the mean-field analysis (i.e., the area between the two dashed lines for $1 < \delta < 3$), we see that the SS phenomenon can be greatly intensified when spatial structure is included. Analogous reasoning applies for region I (green). (For the parameter values used, however, this reasoning does not apply for $\delta > 3$, since in this case the area between the dashed lines can be arbitrarily large. Also we no longer have a region analogous to region II with species A only.) In this way we see that the phase diagram for the spatial stochastic model is rather different from that found in [1]. Moreover, under certain conditions, the survival of the scarcer phenomenon is strengthened.

4 Simulations

Since the preceding analysis involves approximations whose reliability is difficult to assess, we perform simulations of a simple lattice model to verify SSS. We consider the following spatial stochastic process, defined on a lattice of L^d sites. Each site i is characterized by nonnegative occupation numbers a_i and b_i for the two species. The organisms (hereafter “particles”) of the two species evolve according to the following rates:

- Particles of either species hop to a neighboring site at rate D .
- Particles of species A(B) reproduce at rate $\lambda_A(\lambda_B)$.
- At sites with two or more A particles, mutual annihilation occurs at rate $\alpha_A a_i(a_i - 1)$, and similarly for B particles, at rate $\alpha_B b_i(b_i - 1)$.
- At sites having both A and B particles, the competitive reaction $B \rightarrow 0$ occurs at rate $\zeta_A a_i b_i$ and the reaction $A \rightarrow 0$ occurs at rate $\zeta_B a_i b_i$.

The model is implemented in the following manner. In each time step, of duration Δt , each process is realized, at all sites, in the sequence: hopping, reproduction, annihilation, competition.

In the hopping substep, each site is visited, and the probability of an A particle hopping to the right (under periodic boundaries) is set to $p_h = D a_i \Delta t / (2d)$. A random number z , uniform on $[0, 1)$ is generated, and if $z < p_h$ the site is marked to transfer a particle to the right. Once all sites have been visited, the transfers are realized. The same procedure is applied, in parallel, for B particles hopping to the right. Subsequently, hopping in the other $2d - 1$ directions is realized in the same manner.

In the reproduction substep, the A particle reproduction probability at each site i is taken as $p_c = \lambda_A a_i \Delta t$. A random number z is generated and a new A particle created at this site if $z < p_c$. An analogous procedure is applied for reproduction of B particles.

In the annihilation substep, a probability $p_a = \alpha_A a_i (a_i - 1) \Delta t$ is defined at each site, and mutual annihilation ($a_i \rightarrow a_i - 2$) occurs if a random number is $< p_a$. Again, an analogous procedure is applied for annihilation of B particles.

Finally, at sites harboring both A and B particles, probabilities $p_A = \zeta_A a_i b_i \Delta t$ and $p_B = \zeta_B a_i b_i \Delta t$ are defined. The process $B \rightarrow 0$ occurs if a random number $z < p_A$, while the complementary process $A \rightarrow 0$ occurs if $p_A \leq z < p_A + p_B$. Note that at most one of the processes ($A \rightarrow 0$ and $B \rightarrow 0$) can occur at a given site in this substep.

The time step Δt is chosen to render the reaction probabilities relatively small. To do this, before each step we scan the lattice and determine the maximum, over all sites, of a_i , b_i , and $a_i b_i$. With this information we can determine the maximum reaction rate over all sites and all reactions. Then Δt is taken such that the maximum reaction probability (again, over sites and reactions) be $1/5$. In this way, the probability of multiple reactions (e.g., two A particles hopping from i to $i + 1$, etc.) is at most $1/25$, and can be neglected to good approximation, particularly in the regime in which occupation numbers are typically small.

We simulate of the process on a ring ($d = 1$) using *quasistationary* (QS) simulations, intended to sample the QS probability distribution [15, 16]. In these studies the system is initialized with one A and one B particle at each site. When either species goes extinct (an absorbing subspace for the process), the simulation is reinitialized with one of the active configurations (having nonzero populations for both species) saved during the run. Following a brief transient, the particle densities fluctuate around steady values. We search for parameter values such that species A is more numerous, despite being much less competitive than species B (i.e., $\zeta_B \gg \zeta_A$).

Given the large parameter space, certain rates are kept fixed in the study: We set $D = \alpha_A = \alpha_B = 1/4$. We use QS simulations as well as spreading simulations [17] to estimate the critical value of λ for single-species survival. In spreading simulations the initial configuration is that of a single site with one particle, and all other sites empty. We search for the value of λ associated with a power-law behavior of the survival probability $P(t)$ and the mean population size $n(t)$. These studies yield $\lambda_c = 1.267(1)$ as the critical point for survival of a single species, i.e., without competition. (Here and in the following, figures in parentheses denote statistical uncertainties in the final digit.) The phase transition is clearly continuous; details on scaling behavior will be reported elsewhere.

In the two-species studies we set $\lambda_A = 1.6$ and $\zeta_A = 0.005$, so that species A is well above criticality but weakly competitive. We then vary λ_B and ζ_B , monitoring the QS population densities ρ_A and ρ_B of the two species, as well as their QS lifetimes, τ_A and τ_B . The latter are estimated by counting the number of times, in a long QS simulation, that one or the other species goes extinct. Survival of the scarcer is then characterized by the conditions $\rho_A > \rho_B$ and $\tau_A < \tau_B$. For the parameter values studied, we observe SSS for $\lambda_B \approx \lambda_c$ and $\zeta_B \gg \zeta_A$. Figure 6 illustrates the variation of the population densities and of the ratio τ_A/τ_B as ζ_B is varied for fixed $\lambda_B = 1.25$, on a ring of 200 sites. In this case, $\rho_A > \rho_B$ throughout the range of interest; the scarcer species, B, survives longer than A for $\zeta_B \geq 0.25$. Figure 7 shows a sample evolution, for $\zeta_B = 2$ and other

parameters as in Fig. 6, illustrating that sites bearing both species are quite rare, occurring at the frontiers between regions dominated by a single species.

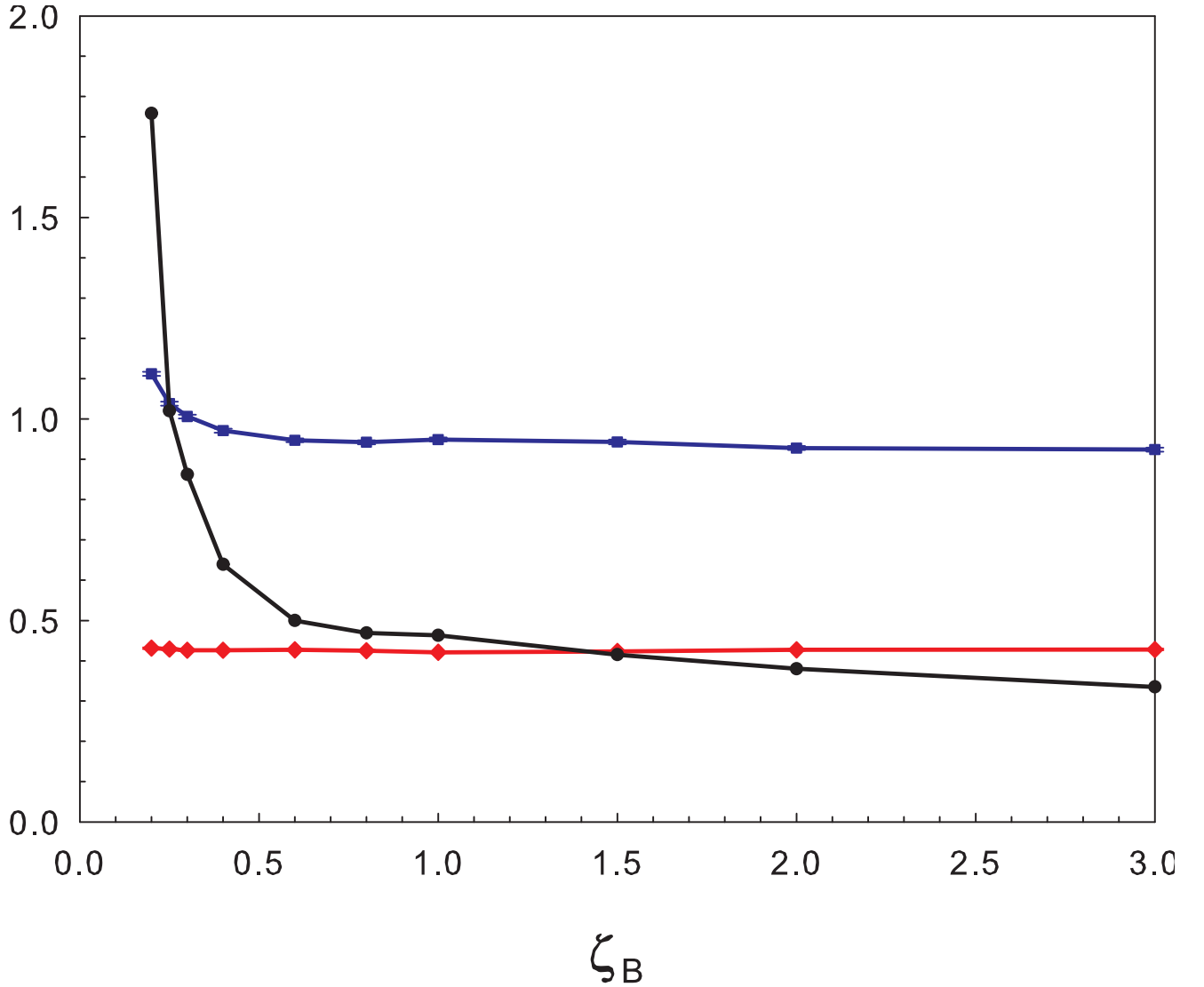


Figure 6: Quasistationary population densities ρ_A (blue) and ρ_B (red), and lifetime ratio τ_A/τ_B (black) versus ζ_B , for parameters as specified in text.

Figure 8 shows the result of a systematic search in the ζ_B - λ_B plane on a ring of $L = 200$ sites. These data represent averages of 200 realizations, each lasting 10^5 time units. SSS is observed in the region bounded by the two curves; the lower curve corresponds to $\tau_A = \tau_B$ while on the upper we have $\rho_A = \rho_B$. Thus SSS is found in a small but significant region of parameter space. Although we use a rather small system to facilitate the search, SSS is not restricted to this system size. For $L = 800$ for example, the range of λ_B values admitting SSS is more restricted (from about 1.24 to 1.27) but at the same time the effect can be more dramatic. For $\lambda_B = 1.27$ and $\zeta_B = 0.2$, for example, we find $\rho_A = 0.74$, $\rho_B = 0.49$, and $\tau_B \approx 100\tau_A$. Thus SSS is observed in simulations of the lattice model. Studies using $\lambda_A = 1.35$ and $\zeta_A = 0.01$ yield a qualitatively similar diagram, leading us to conjecture that the form of the region exhibiting SSS in one dimension is generically that shown in Fig. 5.

In the inset of Fig. 8 the data are plotted in the δ - λ_B plane, for comparison with the theoretical predictions shown in Fig. 5. The region exhibiting SSS is rather different from the predictions of both MFT and stochastic

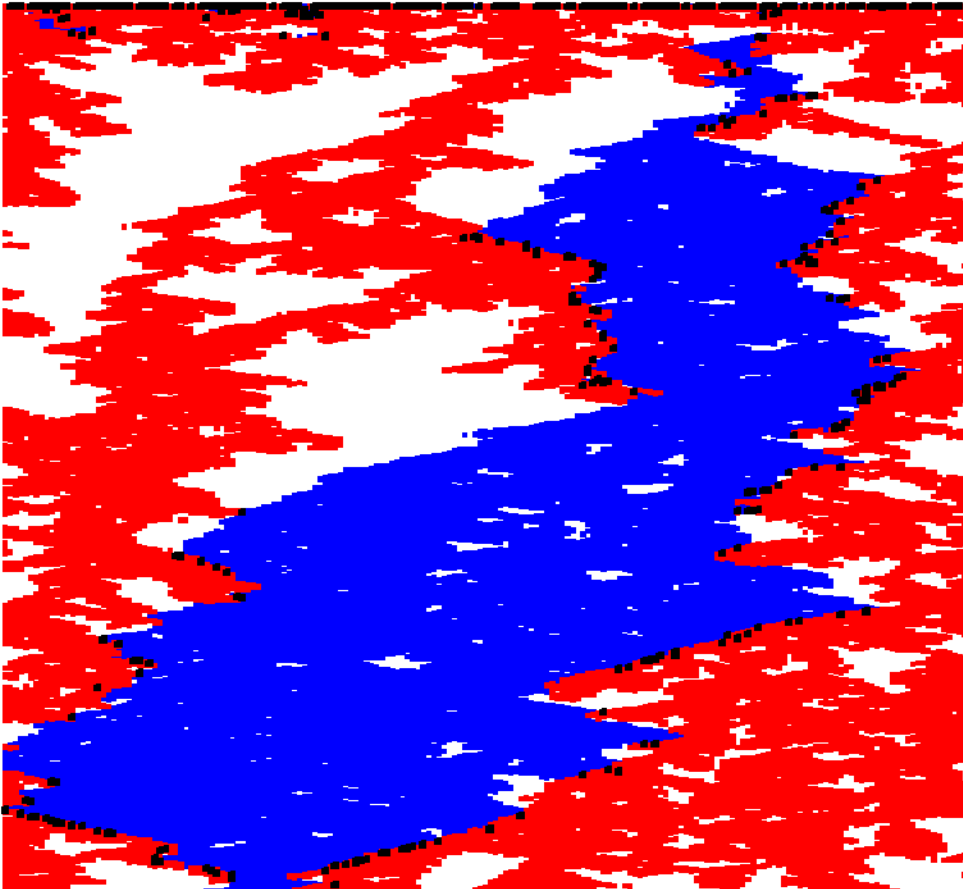


Figure 7: A sample evolution on a ring of 200 sites, of duration 4000 time units (with time increasing downward). Blue: sites with $a_i > 0$ and $b_i = 0$; red: sites with $a_i = 0$ and $b_i > 0$; black: sites with both species present.

field theory. In particular the lower boundary in the δ - λ_B plane is not horizontal and it is unclear whether the SSS region extends to $\delta = 1$. (As λ_B is increased, SSS is observed in an ever more limited range of ζ_B values, making numerical work quite time-consuming.) Here it is important to recall that irrelevant terms (in the renormalization group sense) are discarded in the theoretical analysis, so that predictions for the phase diagram are only qualitative. More detailed simulations, including other parameter sets, larger systems, and simulations on the square lattice, are planned for future work.

5 Conclusion

We study a spatial stochastic model of two-species competition, inspired by the spatially uniform system analyzed in Ref. [1]. Based on Janssen's results of for multicolored directed percolation [7], we find that the flow of parameters under the renormalization group is such that a small competitive advantage may be amplified to the point of excluding the less competitive species, unless the latter reproduces rapidly. Thus the less competitive population can go extinct, regardless of its size as given by mean-field theory. These effects tend to be stronger, the smaller the dimensionality d of the system. Our result shows that the survival of the scarcer phenomenon observed in [1] persists, in some cases in a stronger form, in the presence of spatial structure. These differences are evident when comparing Figs. (1) and (5).

Monte Carlo simulations of a one-dimensional lattice model verify the existence of SSS when the more competitive species has a reproduction rate near the critical value, while that of the less competitive one is

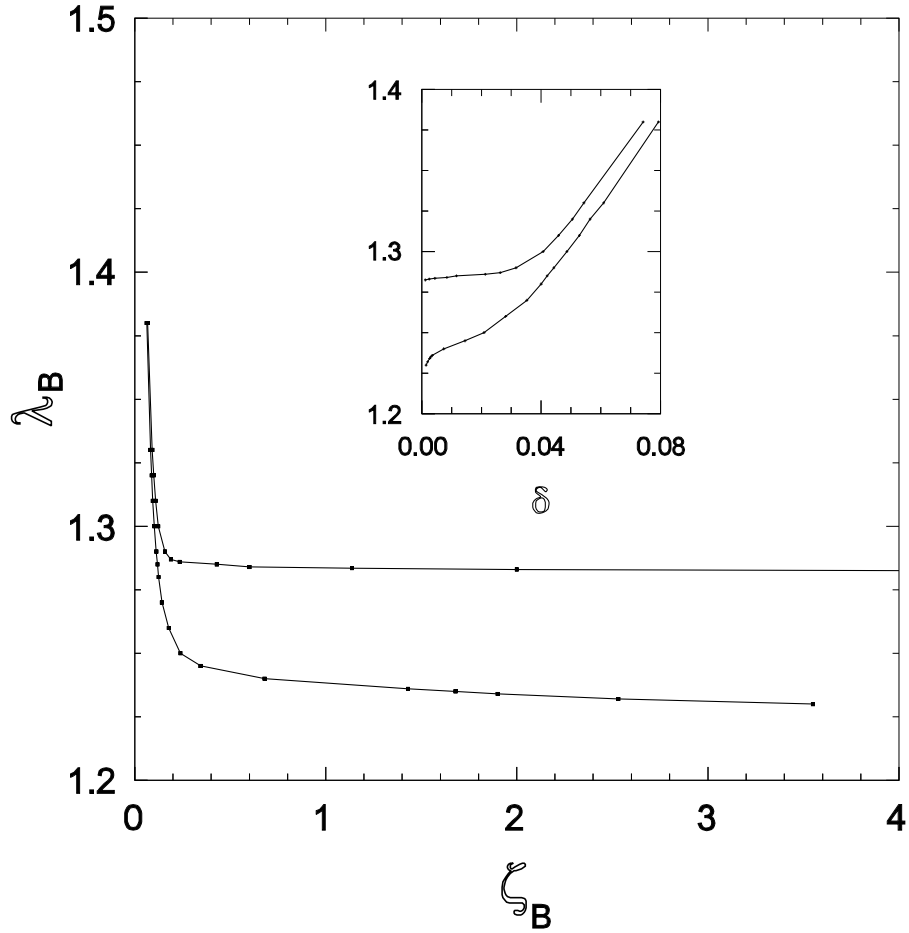


Figure 8: Simulations in one dimension: SSS is observed in the region bounded by the two curves; see text for parameters. Inset: the same data plotted using $\delta = \zeta_A/\zeta_B$ instead of ζ_B on the horizontal axis.

above criticality.

Acknowledgements

This work is supported by CNPq, Brazil.

References

- [1] Gabel, A., Meerson, B., and Redner, S. Jan 2013 *Phys. Rev. E* **87**, 010101.
- [2] Assaf, M. and Meerson, B. (2006) *Phys. Rev. E* **74**(4), 041115.
- [3] Assaf, M. and Meerson, B. (2010) *Phys. Rev. E* **81**(2), 021116.
- [4] Doi, M. (1976) *J Phys A-Math Gen* **9**(9), 1479.
- [5] Peliti, L. (1985) *J. Physique* **46**, 1469.

- [6] Täuber, U. C. (2007) Field-theory approaches to nonequilibrium dynamics In *Ageing and the Glass Transition* pp. 295–348 Springer.
- [7] Janssen, H. (2001) *J Stat Phys* **103(5)**, 801–839.
- [8] Täuber, U. C., Howard, M., and Vollmayr-Lee, B. P. April 2005 *J Phys A-Math Gen* **38(17)**, R79–R131.
- [9] Hochberg, D., Lesmes, F., Morán, F., and Pérez-Mercader, J. Dec 2003 *Phys. Rev. E* **68**, 066114.
- [10] Dennis, G., Hope, J., and Johnsson, M. (2012) *Comput Phys Commun*.
- [11] Dickman, R. (1994) *Phys. Rev. E* **50(6)**, 4404.
- [12] Moro, E. (2004) *Phys. Rev. E* **70(4)**, 045102.
- [13] Dornic, I., Chaté, H., and Muñoz, M. A. (2005) *Phys. Rev. Lett.* **94**, 100601.
- [14] Hinrichsen, H. (2000) *Adv Phys* **49**, 815.
- [15] De Oliveira, M. M. and Dickman, R. (2005) *Phys. Rev. E* **71(1)**, 016129.
- [16] Dickman, R. and Martins deOliveira, M. (2005) *Physica A* **357(1)**, 134–141.
- [17] Grassberger, P. and De La Torre, A. (1979) *Ann Phys-New York* **122(2)**, 373–396.